Faster R-CNN-based Decision Making in a Novel Adaptive Dual-Mode Robotic Anchoring System *

S. Shahin, R. Sadeghian, S. Sareh, *Member, IEEE*

Abstract— **This paper proposes a novel adaptive anchoring module that can be integrated into robots to enhance their mobility and manipulation abilities. The module can deploy a suitable mode of attachment, via spines or vacuum suction, to different contact surfaces in response to the textural properties of the surfaces. In order to make a decision on the suitable mode of attachment, an original dataset of 100 images of outdoor and indoor surfaces was enhanced using a WGAN-GP generating an additional 200 synthetic images. The enhanced dataset was then used to train a visual surface examination model using Faster R-CNN. The addition of synthetic images increased the mean average precision of the Faster R-CNN model from 81.6% to 93.9%. We have also conducted a series of load tests to characterize the module's strength of attachments. The results of the experiments indicate that the anchoring module can withstand an applied detachment force of around 22N and 20N when attached using spines and vacuum suction on the ideal surfaces, respectively.**

I. INTRODUCTION

The development of robotic anchoring systems with the ability for stable mooring and maintaining attachment while transferring across porous and impermeable surfaces is invaluable for a wide range of industrial applications. This might include attachment by climbing robots for inspection and maintenance of buildings including heritage locations, power plants and bridges, and disaster zones [1].

Anchoring into well-grounded structures is a biological approach for locomotion, stiffness control, object manipulation, standing against fluid flows and energy management in animals [1]. Using claws [2], small-scale fibers which can produce adhesion through van der Waals forces [3,4], curling around and enclosing [5,6] or providing negative pressure [1,7] are some of mechanisms that animals, insects or plants use to anchor to their environment. Animals as small as insects and as large as bears use spines or claws to enable interlocking on to the surfaces when climbing [8], where larger animals typically have much blunter claws and therefore poorer attachment ability than smaller animals [8,9]. A complex structures of multilevel branching fibers with specialized tips allow geckos to adhere to almost any surface using van der Waals forces, no matter how slippery [9]. Flying snakes can anchor their selves by wrapping around tree branches [10]. Similarly, tendrils are used by climbing plants, e.g. cucumber, for support and attachment, generally by twining around suitable hosts [6,11]. Octopus arms are equipped with one or two rows of suckers that are controlled independently and can enable multiple functionalities

including anchoring the body to hard substrates by which standing against storm surge and waves [1].

Figure 1. Adaptive vision-based dual-mode anchoring module that can deploy a suitable mode of attachment (spines or vacuum suction) in response to variations in textural properties of the contact surface. Here, the module is attached to a non-living piece of a tree.

Some animals exploit a combination of different mechanisms to attach to the environments. For example, cockroaches can climb an impressive range of materials by using their claws in conjunction with sticky metatarsal pads [8]. Frogs can land and stick on leaves with wet adhesion using peg-like projections and adhesive pads [10]. The tapeworm *Taenia Solium* (parasite of the human gut) uses four suckers around the head to approach the gut wall and a set of hooks to fix onto it [12].

There has been a considerable attention in the literature to the link between the size and weight of animals and their methods and strategies for anchoring to the environment. While smaller insects typically use a combination of spines and adhesive pads for attachment on vertical surfaces, larger animals such as octopus and birds predominantly use suction mechanisms and claws for attachment, respectively [10, 13].

A number of researchers have developed attachment devices based on claws, spines, and suction mechanisms. These include, for example, an omni-directional anchoring foot mechanism based on microspines, hierarchical arrays of claws with suspension flexures, that can tolerate forces as large as 100 N on natural rock surfaces [14]. In [15] an array of independently compliant rotary microspines on a wheel structure was developed that enables the robots to climb rough vertical walls [15].

* S. Shahin, R. Sadeghian, and S. Sareh are with RCA Robotics Laboratory, Royal College of Art, London, UK. (corresponding author: sina.sareh@rca.ac.uk).
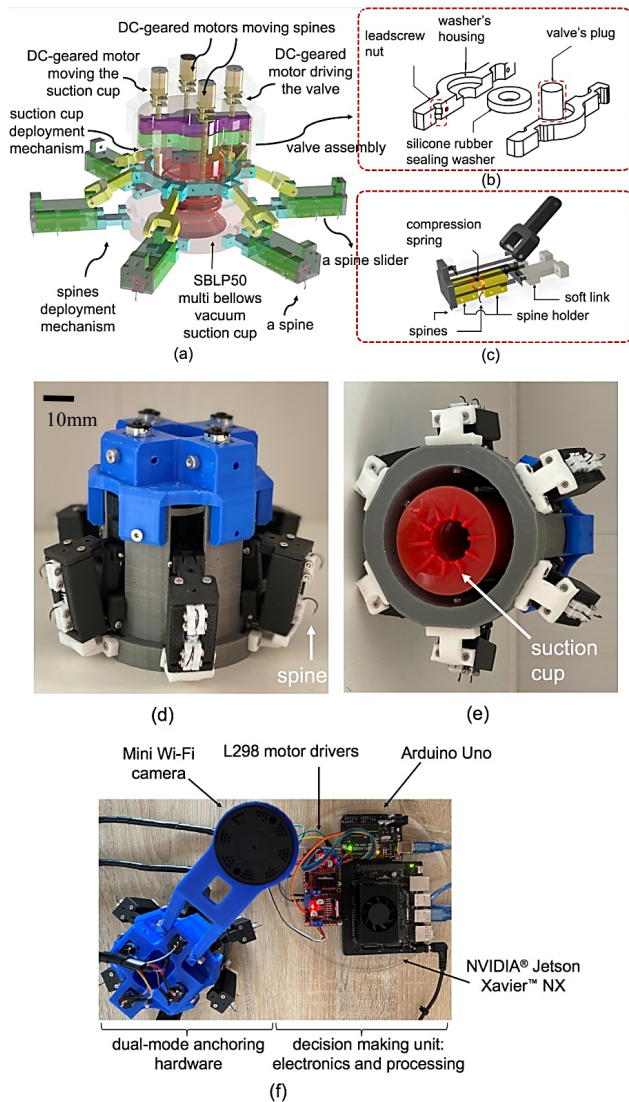
Figure 2. Structure of the dual-mode anchoring module: (a) the configuration of the module when spines are deployed, (b) the structure of the valve used in vacuum suction mode, (c) the spines' deployment mechanism, (d,e) side and bottom views of the module when none of the attachment modes are active, and (f) the anchoring module together with its electronics and processing unit.

The versatility of octopus suckers has also inspired the development of artificial counterparts of this natural organ. This includes the development of artificial suckers actuated by negative air pressure [7], positive air pressure [16], shape memory alloy [17], and dielectric elastomer actuators [18].

There have been some efforts on combining different modes of attachment. In [19], a self-aligning gripper based on combining gecko-like and electrostatic adhesive mechanisms is proposed, where the two modes of attachment complement each other; while the gecko-like adhesives can typically provide high adhesion force to smooth surfaces with limited ability for attachment to rough surfaces, the electrostatic adhesives that can enable attachment to a wider range of materials at a lower level of adhesion. In [20], a worm-inspired wall-climbing robot utilizing an anchoring mechanism based on the composition of suckers and microspines is proposed; their experimental tests on the

sucker-microspine composite structure shows an increase in the frictional resistance on rougher wall surface by about 30% compared with the traditional pure suction cup structure. These approaches were based on concurrent activation of all two modes of attachment aiming at increasing the chance or strength of attachment by using a combination.

However, in many applications, the use of certain modes of attachment can be ineffective or even harmful. For example, the activation of vacuum pressure-based suction cups on porous surfaces can be very inefficient, ineffective, and wasteful in terms of the robot's energy management. Similarly, the activation of artificial spines on delicate contact surfaces can damage the contact surface. In order to avoid this, the attachment system should adapt effective methods to attach to different contact surfaces taking into account the respective surface properties. This requires different modes of attachment to be deployable independent of each other, as opposed to their simultaneous deployment [1].

Hence, in this paper, we propose a dual-mode anchoring module that can switch between vacuum suction and spine attachment based on the surface properties of the environment, Fig.1. The contributions of this paper can be summarized as follows:

1. Creating an anchoring module with independently deployable mechanisms for vacuum suction and spine attachment.

2. Designing a Faster Region-based Convolutional Neural Networks (Faster R-CNN) algorithm to detect the surface properties of the environment that the robot is interacting with, using an integrated Wi-Fi camera, and optimization of the relevant code for implementation on an NVIDIA Jetson Xavier NX, as the processing unit. This arrangement provides the possibility of autonomous decision making on the suitable mode of attachment to the environment.

The contact surfaces studied are mainly those found in natural environments including rocks and cliffs, various tree trunks and muddy surfaces, in addition to some indoor features. For the purpose of training by deep learning methods, a rich dataset of fully-textured images was required. In order to enhance our dataset of the relevant images, the Wasserstein Generative Adversarial Network with Gradient Penalty (WGAN-GP) was used to create a synthetic dataset of 200 images. Subsequently, a Faster R-CNN algorithm was used to train the system to enable a fully automated visual examination of surface textures.

The remainder of this paper is organized as follows. In Section II, our approach in the development of the dual-mode anchoring hardware is described. In Section III, various methods of generating synthetic data are studied, and WGAN-GP was selected for generating additional synthetic images. The image pre-processing approach used in this study is also explained in this section, and finally, a model for detecting textural properties of contact surfaces was created using Faster R-CNN. The experimental testing of the anchoring module and respective results constitute Section IV. The conclusions and future works are presented in Section V.

II. Dual-mode anchoring module Hardware

The dual-mode anchoring module contains two attachment mechanisms using spines and vacuum suction, Fig. 2. The spines are used to attach to porous surfaces, such as resin-bound driveways and certain types of buildings' facades, and the vacuum suction system is used to attach to a range of non-porous and smooth surfaces such as the window glass. The weight of the module is 0.375 kg, excluding its processing unit. In the following, the process of design, fabrication, and testing of each attachment mechanism is described.

A. Attachment with Vacuum Suction

The vacuum suction attachment mechanism is comprised of a multi bellows vacuum suction cup, a bespoke valve mechanism integrated with the cup, and two motorized sliders that enable moving the cup and the valve's plug independently in a perpendicular direction to the surface, as shown in Fig. 2. The suction cup used in this study is a SBLP50 (VACUFORCE, USA).

The valve mechanism is comprised of a rigid plug, a washer made of soft silicone rubber (Mold Max 14NV, Smooth-On, USA) used for sealing, and a DC-geared motor with leadscrew to move the valve's plug, as described in Fig. 2a, b. The valve's plug is used to block the suction cup inlet when the cup is compressed. This creates a negative pressure inside the cup enabling attachment.

B. Attachment with Spines

In order to construct a spine mechanism, we used standard fishing hooks (Crivit leader and hook set, size 8). Each hook is integrated with a retraction mechanism (a spine holder and a compression spring) forming a retractable spine. Every two retractable spines are then integrated into a toe-like housing connected to the anchoring modules external body using a rigid link at the top and a soft link at the bottom, as presented in Fig. 2a, c. The toe-like housing structure, retraction mechanism, and sliders are fabricated using Onyx materials via a Mark 2 3D printing machine, Markforged, USA. The use of a soft link in the construction of the spine deployment mechanism enables the elastic deployment of the spines over the contact surface leading to better engagement between the spines and dips and bumps of the contact surface. Hence, a soft link was fabricated from Ecoflex 00-30 super-soft silicone rubber, Smooth-On, USA, as shown in Fig. 2c.
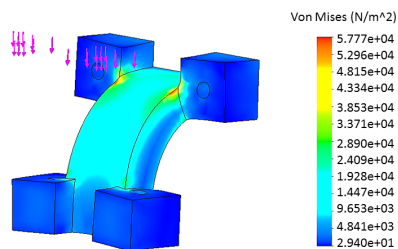

Figure 3. The stress analysis of the soft link indicating that the link will not fail under a tensile force of up to 5N.

As the anchoring module should be able to hold a load of up to 30N and we have six toe-like housing for spines, each soft link should be able to hold up to 5N. In order to evaluate the effectiveness of the proposed soft links a finite element (FE) model of the link was produced in SolidWorks® Simulation. The Young module and Poisson ratio of Ecoflex 00-30 used in the construction of the link are 170 Pa and 0.49, respectively [21-22]. Figure 3 shows the stress analysis of the soft link, indicating that under a maximum load of 5N, the soft link is still stable.

C. The module's electronics and processing unit

The electronics and processing unit of the module is in charge of the processing of images from the contact surface, subsequent decision making on deployment of a suitable mode of attachment, and generating relevant control signals for motor drivers. As it is shown in Fig. 2f, an NVIDIA Jetson Xavier NX is used as the main control board and an Arduino Uno works as the interface between the motor drivers and the NVIDIA Jetson Xavier NX.

III. Visual Examination of surface properties to make decision on the suitable mode of attachment

In order for the dual-mode anchoring module to deploy the suitable mode of attachment, it should be provided with textural information of the contact surface. Hence, in this study, an algorithm based on Faster R-CNN is designed and implemented on an NVIDIA Jetson Xavier NX, within the electronics and processing unit of the module. The algorithm is designed based on the fit for attachment using spines. This arrangement enables answering the question that whether the specified region is suitable for attachment using spines; if the answer is 'no' then the vacuum suction mode is deployed. Note that, the main reason for choosing the Faster R-CNN algorithm was the ability to run this type of algorithm on NVIDIA Jetson Xavier NX with low latency at a high precision [23]. The design and implementation process of the proposed algorithm can be summarized as follows:

(1) A dataset of 100 images from environments that are suitable for attachment via spines is created through photography.

(2) All images within the dataset are labeled and then relevant TFRecords files are generated for training a model based on the Faster R-CNN algorithm. The mean average precision of the trained model was calculated as 81.6%.

(3) In order to improve the precision of the trained model, a WGAN-GP was designed and applied to the preliminary dataset to generate new members for the dataset, thereby creating a new dataset of 300 images, including the original images. The improved mean average precision of the trained model with the new dataset was then calculated as 93.9 %. It should be noted that the calculations were based on 1000 training iterations.

Figure 4 presents eight members of the dataset gathered based on the fit for spine attachment. Increasing the number of dataset members has a direct effect on the Faster R-CNN's model precision which improves the surface examination accuracy.

A. Generating Data with WGAN-GP

According to [24], the GAN is structured from two networks, a generator network to generate synthetic images from an original input dataset, and a discriminator to determine the similarity between the produced synthetic image and the real ones. A synthetic image can be added to the original dataset if the discriminator detects it as a real image.
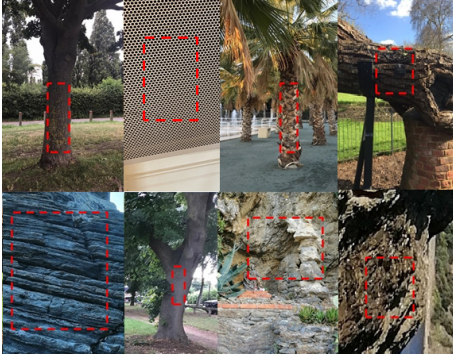
Figure 4. Example members of the dataset gathered based on the fit for spine attachment.

The relation between the generator and discriminator of a GAN framework can be presented as a min-max structure as follows:

$$\min_{G} \max_{D} \mathbb{E}[\log(D(x))] + \mathbb{E}[1 - \log(D(\tilde{x}))] \quad (1)$$
$$x \sim P_r \qquad \tilde{x} \sim P_g$$

where,

$$\tilde{x} = G(z), \qquad z \sim p(z) \quad (2)$$

In Eq. 1, P_r and P_g denote as the original data distribution and the synthetic data distribution which are implicitly defined by Eq. 2. Moreover, $\mathbb{E}$ and D are defined as the expected value and discriminator's estimation function, respectively. The z variable in Eq. 2 represents a noise sample distribution, which is used as the input of the generator. Note that z can be sampled from noise distributions such as the Gaussian or uniform distributions. However, based on [25], [26], and [27], the training of GAN is unstable due to the gradient vanishing, if the discriminator is optimally trained. In order to solve this issue, in [28], a solution by using Earth-Mover (also called Wasserstein-1) distance is proposed, known as WGAN. By using Kantorovich- Rubinstein duality [29], the value function of the WGAN can be obtained as follows:

$$\min_{G} \max_{D \in S} \mathbb{E}[D(x)] + \mathbb{E}[D(\tilde{x})] \quad (3)$$
$$x \sim P_r \qquad \tilde{x} \sim P_g$$

where S is a set of 1-Lipschitz function. According to Eq. 3, by using an optimal discriminator, named 'critic' in [30], to minimize the value function $W(P_r, P_g)$, the generator parameter should be minimized. In [30], a method of weights clipping of the critic within $[-c, c]$, where c is the clipping parameter, to enforce the Lipschitz constraint on the critic is proposed. However, the proposed solution can lead to an explosion gradient problem [30].

In order to solve the aforementioned problems, in [24], an alternative solution, known as WGAN-GP, to enforce the Lipschitz constraint by directly constraining critic's output gradient norm in respect of its input is proposed,

$$x_r \sim p_r, x_g \sim p_g, \epsilon \sim Uniform[0,1] \quad (4)$$
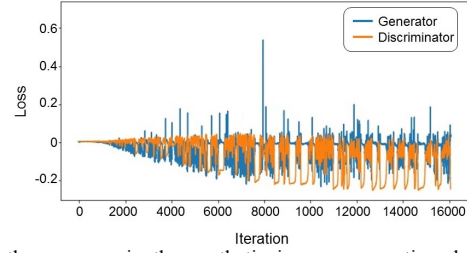

Figure 5. the progress in the synthetic images generation during 16000 iterations of WGAN-GP.

Based on Eq. 4, a real sample (x_r) and a fake samples (x_g) are randomly taken from the original dataset and the generator, respectively. Then a random number between 0 and 1 is chosen, to define the random samples using the following function:

$$\tilde{x} = \epsilon x_r + (1 - \varepsilon) x_g \quad (5)$$

Moreover, based on [24], in order to fulfill the WGAN-GP conditions, the loss of critic should be transformed to:

$$L = -\mathbb{E}[D(x)] + \mathbb{E}[D(\tilde{x})] + \lambda \mathbb{E}[(\|\nabla_{\hat{x}} D(\hat{x})\|_2 - 1)^2] \quad (6)$$
$$x \sim P_r \quad \tilde{x} \sim P_g \qquad \hat{x} \sim P_{\hat{x}}$$

where λ and $\hat{x}$ are the gradient penalty coefficient and random samples based on P_r and P_g. The applied WGAN-GP algorithm is based on Tensorflow and Keras. The preliminary dataset used to generate synthetic images includes 100 images with a size of 256x256. The Adam optimizer is applied to the WGAN-GP, where its hyper-parameters, α, β, γ, and ε are valued as, 0.001, 0, 0.9 and 10^{-8}. The gradient penalty coefficient and the number of critic iterations per generator iteration are 10 and 5 based on [24], respectively.
In this study, 200 images were generated using the WGAN-GP algorithm. Figure 5 illustrates the progress in the synthetic generation of images during 16000 iterations.

B. Labeling & Generating TFRecords

In order to label the dataset members, the labelImg software [31] was used. Using the LabelImg software the bounding box and images annotation files were prepared. Then, the preliminary labeled dataset was divided into two parts: train and test, with a ratio of 80% and 20% in terms of the number of members. To store the images as a sequence of binary records, they were converted to TFRecord format, where the TFRecord is the input of the surface examination training system. Following the preparation, the Faster R-CNN algorithm is used to train the surface visual examination model.

C. Faster R-CNN

The designed Faster R-CNN has two main parts, a Region Proposal Network (RPN), and a Region Detection Network (RDN). The RPN is used for ranking the region boxes, which are called anchors. The RPN ranking is based on similarity approximation of the environment considered for attachment and the trained model by using a classifier and

a regressor. The RPN labels the anchors with higher overlaps with the ground truth anchors as foreground, and the other ones as background. RDN is used to detect objects.

The labeled anchors will be fed into the *softmax* logistic regression activation function to detect the labels. Based on [32], the RPN loss function can be expressed as:

$$L(\{p_i\}, \{t_i\}) = \frac{1}{N_{cls}} \sum_i L_{cls}(p_i, p_i^*) + \lambda \frac{1}{N_{reg}} \sum_i p_i^* L_{reg}(t_i, t_i^*) \quad (7)$$

where

$$L_{reg}(t_i, t_i^*) = R(t_i, t_i^*) \quad (8)$$
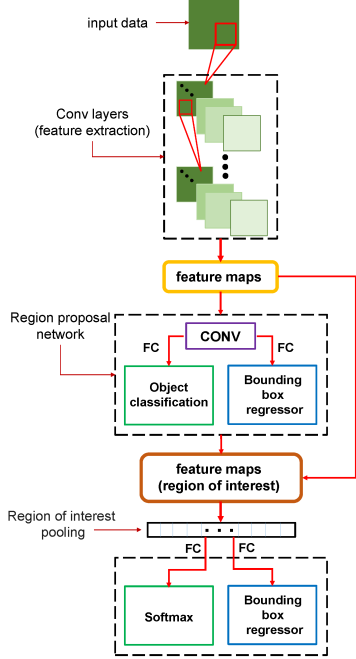
Figure 6. The structure of our Faster R-CNN algorithm. Note that FC and CONV represent Fully Connected and Convolutional layers, respectively.
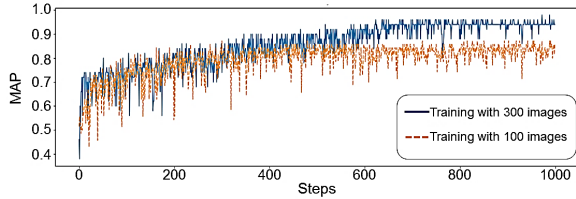

Figure 7. The improvement of Faster R-CNN's Mean Average Precision (MAP) by adding the 200 synthetic images obtained using WGAN-GP.

In Eq. 7, i denotes an anchor index in a mini-batch, P_i is the possibility for the predicted anchor i to be a suitable region for anchoring with spines, and P_i^* is ground truth which should be one if the anchor is "positive" and zero if the anchor is "negative"[33]. Moreover, t_i is a vector containing the predicted bounding box with four parameterized coordinates, and t_i^* is the ground truth box related with a positive anchor, and L_{cls} is the log loss obtained based on the prepared area for attachment is detected or not. In Eq. 8, L_{reg} and R represent the regression loss and robust loss functions as presented in [34], respectively. In Eq.7, when the anchor becomes positive then P_i will be one and the regression will be active, vice versa if the value of P_i^* is zero, the regression will be disabled.
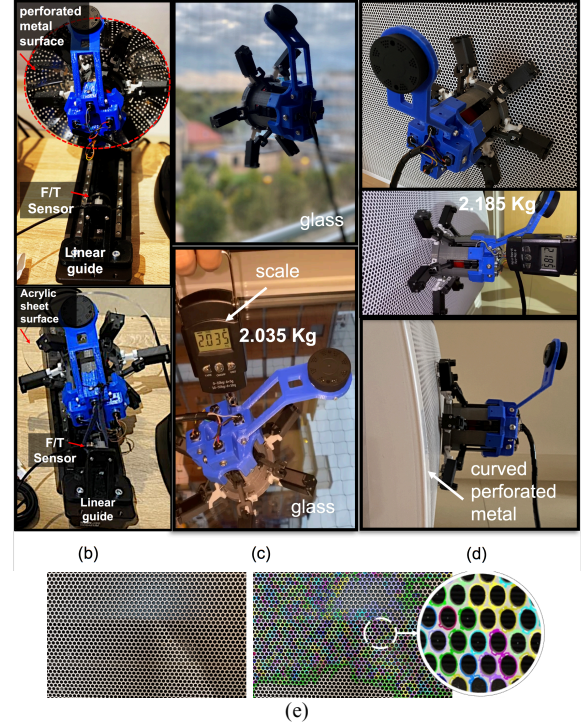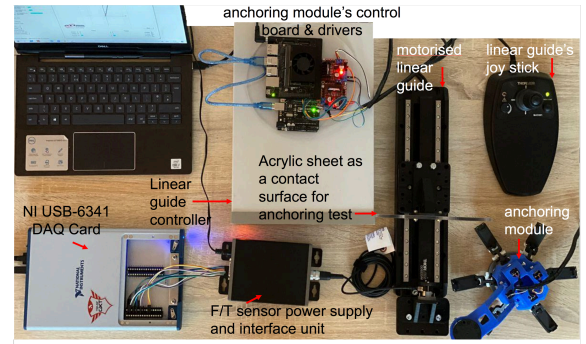

Figure 8. (a) The configuration of the experimental setup to measure anchoring strength (load testing). A motorised linear guide was used to move various contact surfaces away from the attached anchoring module, while the module was mechanically linked to a Nano17 F/T Sensor, (b) anchoring module attached to a perforated metal surface using spines for the purpose of load testing (top panel), and anchoring module attached to an acrylic sheet using vacuum suction for lead testing (bottom panel), (c) anchoring module is attached to the window's glass using vacuum suction can withstand an applied detachment force of around 20N, (d) anchoring module is attached to a curved perforated metal surface using spines can withstand an applied detachment force of around 22N, (e) visual surface examination output for a perforated metal surface, based on the Faster R-CNN model.

Eq. 7 presents the output of the classification and regression layers, normalized with N_{cls} and N_{reg} respectively, and λ is a balancing weight. The next step after applying the RPN is to reduce the feature map by using the Region of Interest (RoI) pooling. The training of the RPN was performed using Stochastic Gradient Descent (SGD) for both classification and regression at the same time jointly. Figure 6 presents our Faster R-CNN algorithm, which is configured based on [33]. By adding the obtained 200 synthetic images from WGAN-GP the training model's mean average precision was increased from 81.6% to 93.9%, based on 1000 training iterations, Fig. 7.

IV. ANCHORING STRENGTH: EXPERIMENTAL LOAD TESTING AND RESULTS

In order to characterize the anchoring strength of the module in different modes, we have conducted a series of load testing experiments using the experimental setup, shown in Fig. 8 comprising a motorized linear guide with a fixed platform that is integrated with a Nano17 F/T Sensor and a moving platforms integrated with different types of contact surface samples. The module is attached to the contact surface during the experiments and is under tensile force, measured by the F/T Sensor, as the distance between the moving and fixed platform changes, Fig. 8. The experimental results show that the module can withstand a pulling force of around 20N and 22N when anchoring using spines and vacuum suction respectively.

V. CONCLUSIONS

This paper presents a dual-mode anchoring module that can be integrated into robots to enhance their mobility and manipulations abilities. The module acquires and processes visual information from the contact surfaces in the environment and deploys a suitable mode of attachment, spine or vacuum suction, depending on the textural properties of the contact surface. In order to make a decision on the suitable mode of attachment, the original dataset of 100 photos was enhanced using a WGAN-GP generating an additional 200 synthetic photos of potential contact surfaces, and then a visual surface examination model was trained using Faster R-CNN. The use of the enhanced dataset increased the mean average precision of the Faster R-CNN model from 81.6% to 93.9%. We conducted a series of load tests to characterize the strength of attachments by the anchoring module. The results of the experiments indicate that the anchoring module can withstand an applied detachment force of around 22N and 20N when attached using spines and vacuum suction, respectively.

REFERENCES

[1] S. Sareh, K. Althoefer, M. Li, Y. Noh, F. Tramacere, P. Sareh, B. Mazzolai, M. Kovac "Anchoring like octopus: biologically inspired soft artificial sucker". Journal of the Royal Society Interface. 2017 Oct 31;14(135):20170395.

[2] A. Sintov, T. Avramovich, A. Shapiro, "Design and motion planning of an autonomous climbing robot with claws", Robotics and Autonomous Systems. 2011 Nov 1;59(11):1008-19.

[3] S. Kim, "Polymer micro/nanofiber arrays with mushroom-shaped tips as gecko foot-hairs inspired adhesives," 2009.

[4] L. Daler, A. Klaptocz, A. Briod, M. Sitti, D. Floreano,"A perching mechanism for flying robots using a fibre-based adhesive", In2013 IEEE International Conference on Robotics and Automation 2013 May 6 (pp. 4433-4438). IEEE.

[5] C. Wright, A. Buchan, B. Brown, J. Geist, M. Schwerin, D. Rollinson, M. Tesch, H. Choset, "Design and architecture of the unified modular snake robot", Proceedings of the IEEE International Conference on Robotics and Automation, St. Paul, USA, 2012, 4347–4354.

[6] I. Must, E. Sinibaldi, B. Mazzolai. "A variable-stiffness tendril-like soft robot based on reversible osmotic actuation", Nature communications. 2019 Jan 21;10(1):1-8.

[7] F. Tramacere, M. Follador, N.M. Pugno, B. Mazzolai, "Octopus-like suction cups: from natural to artificial solutions", Bioinspiration and Biomimetics 10: 035004. (doi: 10.1088/1748-3190/10/3/035004).

[8] W. Provancher, J. Clark, B. Geisler, M. "Cutkosky,Towards Penetration-based Clawed Climbing". 10.1007/3-540-29461-9_94, 2005.

[9] J.G. Pattrick, D. Labonte, W. Federle, "Scaling of claw sharpness: mechanical constraints reduce attachment performance in larger insects", Journal of Experimental Biology 2018 221: jeb188391.

[10] W.R. Roderick, M.R. Cutkosky, D. Lentink, "Touchdown to take-off: at the interface of flight and surface locomotion". Interface focus. 2017

[11] S. Sareh *et al.*, "Bio-inspired tactile sensor sleeve for surgical soft manipulators," *2014 IEEE International Conference on Robotics and Automation (ICRA)*, Hong Kong, 2014, pp. 1454-1459.

[12] K. Willms, "Morphology and biochemistry of the pork tapeworm, Taenia solium", Current Topics in Medicinal Chemistry, 8(5), 375–382.

[13] M. KOVAC, Learning from nature how to land aerial robots, *SCIENCE*20 MAY 2016: 895-896.

[14] A. Parness, "Anchoring foot mechanisms for sampling and mobility in microgravity". In2011 IEEE International Conference on Robotics and Automation 2011 May 9 (pp. 6596-6599). IEEE.

[15] K. Carpenter, N. Wiltsie, A. Parness, "Rotary microspine rough surface mobility". IEEE/ASME Transactions on Mechatronics. 2015 Dec 23;21(5):2378-90.

[16] Y. Tang, Q. Zhang, G. Lin, J. Yin, "Switchable adhesion actuator for amphibious climbing soft robot" Soft robotics.2018 1;5(5):592-600.

[17] B. Hu, L. Wang, Z. Fu, Y. Zhao, "Bioinspired miniature suction cups actuated by shape memory alloy". International Journal of Advanced Robotic Systems. 6(3), 151–160, 2009.

[18] M. Follador, F. Tramacere, B. Mazzolai, "Dielectric elastomer actuators for octopus inspired suction cups". Bioinspiration and Biomimetics, 9(4): 046002, 2014. (doi: 10.1088/1748-3182/9/4/046002).

[19] M. Dadkhah, *et al*, "Self-aligning gripper using an electrostatic/gecko-like adhesive". In 2016 IEEE/RSJ IROS pp. 1006-1011.

[20] W. Yang, C. Yang, R. Zhang, W. Zhang, "A Novel Worm-inspired Wall Climbing Robot with Sucker-microspine Composite Structure", In2018 3rd International Conference on Advanced Robotics and Mechatronics (ICARM) 2018 Jul 18 (pp. 744-749). IEEE.

[21] J.L Sparks, N.A. Vavalle, K.E. Kasting, B. Long, M.L. Tanaka, P.A. Sanger, K. Schnell, T.A. Conner-Kerr, "Use of silicone materials to simulate tissue biomechanics as related to deep tissue injury", Advances in skin & wound care. 2015 Feb 1;28(2):59-68.

[22] Y. Fouillet, C. Parent, G. Gropplero, L. Davoust, J.L. Achard, F. Revol-Cavalier, N. Verplanck, "Stretchable material for microfluidic applications", InMultidisciplinary Digital Publishing Institute Proceedings 2017 (Vol. 1, No. 4, p. 501).

[23] M. Vandersteegen, K. Van Beeck, T. Goedemé, "Super accurate low latency object detection on a surveillance UAV". In2019 16th International Conference on Machine Vision Applications (MVA).

[24] I. Gulrajani, F. Ahmed, M. Arjovsky, V. Dumoulin and A.C. Courville, "Improved training of wasserstein gans", In Advances in neural information processing systems, pp. 5767-5777, 2017.

[25] I. Goodfellow, NIPS 2016 tutorial: Generative adversarial networks, arXiv preprint arXiv:1701.00160, 2016.

[26] J.T. Wang and C.H. Wang, "High Performance WGAN-GP based Multiple-category Network Anomaly Classification System", In 2019 International Conference on Cyber Security for Emerging Technologies (CSET), pp. 1-7, IEEE, 2019.

[27] W. Fu, D. Zhang, Y. Fu, J. Li, and Y. Xie, "Arrears prediction for electricity customer through Wgan-Gp", In 2017 IEEE 2nd Information Technology, Networking, Electronic and Automation Control Conference (ITNEC) pp. 1667-1670, IEEE, 2017.

[28] M. Arjovsky, L. Bottou, "Towards principled methods for training generative adversarial networks", preprint arXiv:1701.04862. 2017.

[29] C. Villani, Optimal transport: old and new., Springer Science & Business Media; 2008 Oct 26.

[30] M. Arjovsky, S. Chintala, L. Bottou, "Wasserstein gan"., arXiv preprint arXiv:1701.07875. 2017 Jan 26.

[31] Tzutalin. LabelImg.Git code (2015) https://github.com/tzutalin/labelImg

[32] S. Ren, K. He, R. Girshick, J. Sun "Faster r-cnn: Towards real-time object detection with region proposal networks", In Advances in neural information processing systems pp. 91-99, 2015.

[33] C. Eggert, S. Brehm, A. Winschel, D. Zecha, R.A. Lienhart "closer look: Small object detection in faster R-CNN". ICME 2017, pp. 421-426.

[34] R. Girshick, "Fast R-CNN", arXiv:1504.08083, 2015.